International Journal of Earth Sciences

Relationship between alternating open/closed conduit conditions and deformation patterns: an example from the Somma-Vesuvio volcano (southern Italy)

--Manuscript Draft--

Manuscript Number:	
Full Title:	Relationship between alternating open/closed conduit conditions and deformation patterns: an example from the Somma-Vesuvio volcano (southern Italy)
Article Type:	Original Paper
Keywords:	volcano-tectonics; structural analysis; DTM lineament analysis; volcanic dykes
Corresponding Author:	Francesco D'Assisi Tramparulo, Ph.D. Istituto Nazionale di Geofisica e Vulcanologia ITALY
Corresponding Author Secondary Information:	
Corresponding Author's Institution:	Istituto Nazionale di Geofisica e Vulcanologia
Corresponding Author's Secondary Institution:	
First Author:	Francesco D'Assisi Tramparulo, Ph.D.
First Author Secondary Information:	
Order of Authors:	Francesco D'Assisi Tramparulo, Ph.D.
	Stefano Vitale, Ph.D.
	Roberto Isaia, Ph.D.
	Alessandro Tadini, Ph.D.
	Marina Bisson, Ph.D.
	Ernesto Paolo Prinzi, Dr
Order of Authors Secondary Information:	
Funding Information:	
Abstract:	With the aim to investigate the relationships between the current deformation setting of the Somma-Vesuvio volcano and its volcano-tectonic evolution, we show the results of a meso-scale systematic structural analysis on fractures, faults and dykes and a macro-scale morphological lineament analysis carried out from high-resolution Digital Terrain Models (DTMs). Fractures include: (i) cooling joints, subsequently reactivated as normal and oblique faults during the caldera collapse episodes; (ii) radial and tangential metric fractures likely associated to volcanic inflaction/deflaction stages and (iii) macro-fractures related to slope instabilities. Dykes occur with different geometries including en-echelon structures bounding grabens. The orientation analysis on all structures marks preferred directions NW-SE, NE-SW, N-S and E-W amongst the dominant ones. Furthermore, azimuth and spatial position of dykes and morphological lineaments were analyzed comparing them with the old Somma volcano and Gran Cono centers, respectively. Results highlight the overprinting of radial and clustered strain patterns recorded in different volcano-tectonic evolution stages: the radial pattern forms during the volcanic inflation with a closed magmatic conduit; on the contrary, the regional strain pattern, characterized by preferred orientation, prevails on the local deformation field in the case of the open conduit activity.

Relationship between alternating open/closed conduit conditions and deformation patterns: an example from the Somma-Vesuvio volcano (souther Italy)

Tramparulo F.D.A.[1], Vitale S.[1-2], Isaia R.[1], Tadini A.[3-4], Bisson M.[4], Prinzi E.P.[2]

[1]Istituto Nazionale di Geofisica e Vulcanologia, sezione di Napoli Osservatorio Vesuviano, Via Diocleziano 328, 80124 Napoli

[2]Dipartimento di Scienze della Terra, dell'Ambiente e delle Risorse (DiSTAR), Università di Napoli Federico II, Largo San Marcellino 10, 80138, Napoli

[3]Dipartimento di Scienze della Terra, Università di Firenze, Firenze, Italy

[4]Istituto Nazionale di Geofisica e Vulcanologia, Sezione Pisa, Pisa, Italy

Corresponding author: francescodassisi.tramparulo@unina.it, tel +39.081.2538124

Keywords: volcano-tectonics, structural analysis, DTM lineament analysis, volcanic dykes.

Abstract

With the aim to investigate the relationships between the current deformation setting of the Somma-Vesuvio volcano and its volcano-tectonic evolution, we show the results of a meso-scale systematic structural analysis on fractures, faults and dykes and a macro-scale morphological lineament analysis carried out from high-resolution Digital Terrain Models (DTMs). Fractures include: (i) cooling joints, subsequently reactivated as normal and oblique faults during the caldera collapse episodes; (ii) radial and tangential metric fractures likely associated to volcanic inflaction/deflaction stages and (iii)

macro-fractures related to slope instabilities. Dykes occur with different geometries including *en-echelon* structures bounding grabens. The orientation analysis on all structures marks preferred directions NW-SE, NE-SW, N-S and E-W amongst the dominant ones. Furthermore, azimuth and spatial position of dykes and morphological lineaments were analyzed comparing them with the old Somma volcano and Gran Cono centers, respectively. Results highlight the overprinting of radial and clustered strain patterns recorded in different volcano-tectonic evolution stages: the radial pattern forms during the volcanic inflation with a closed magmatic conduit; on the contrary, the regional strain pattern, characterized by preferred orientation, prevails on the local deformation field in the case of the open conduit activity.

1. Introduction

Defining deformation structure patterns in the volcanic edifices is a useful tool for disclosing the stress field acting during the volcano activity and the role of the local stress field with respect to the regional deformation pattern (e.g. Gudmundsson, 1995; Marinoni and Gudmundsson, 2000; Pollard et al., 1983). Volcanoes characterized by a well-defined central conduit, such as the Somma-Vesuvio (SV), are mainly characterized by radial deformation patterns of faults, fractures, dykes and eruptive fissures (e.g. Acocella and Neri, 2009; Vezzoli et al., 2014) usually resulting from uniform stress fields, whose symmetry is a consequence of the stress focusing above the magma chamber center. According with several authors (e.g. McGuire and Pullen, 1989; Pinel and Jaupart, 2003) the main factor driving this phenomenon is the edifice load. However, stress focusing is also controlled by the presence of a well-localized central conduit that at SV is well-defined by geophysical surveys (Di Stefano and Chiarabba, 2002; Zollo et al., 2002; De Natale et al., 2004). Nevertheless, discrepancies from this simple model can exist. A strong tectonic stress field can considerably modify the radial pattern (e.g. Muller and Pollard, 1977; Nakamura, 1977; Odé, 1957), for example in the case of synchronous activity of a volcanic radial pattern and a well-marked regional deformation field, the resulting strain field is a complex array of structures that can be disclosed by means of specific orientation analyses that separate radial and unidirectional components (e.g. Quintà et al. 2012). In others cases the occurrence of mega-landslides (Becerril et al., 2015) or preexisting anisotropies in the host rock (Gudmundsson, 2006) can locally mask the radial pattern. In the case of SV, a local variation of the radial pattern could result by the active gravitational spreading triggered by the edifice load and the occurrence of a weak sedimentary layer underlying the volcano (e.g. Borgia et al., 2005; Marturano et al., 2009; D'Auria et al., 2014) or by flank failures (e.g. Ventura et al., 1999).

This paper aims to provide a complete framework of the deformation state of the SV volcano, by means of a multi-scale approach that combines the orientation analysis of fractures, faults, dykes (collected during several field surveys), and the analysis of morphological lineaments derived after

the inspection of high-resolution Digital Terrain Models (DTMs). This study allowed us to shed light on the connection between the current deformation pattern and the complex tectonic and eruptive history of the volcano, characterized by Plinian to effusive eruptions and alternating open and closed conduit stages.

2. Geological setting

The SV volcano is located in the southern sector of the Campanian Plain (Fig. 1), a structural depression filled by Pleistocene to Holocene continental, volcanic and marine deposits, bounded to SE, E and NE by several Meso-Cenozoic carbonate ridges (e.g. Santangelo et al., 2010 and references therein). The SV is a stratovolcano ~1300m high formed by lavas, scoriae and pyroclastic depositsincluding ultrapotassic to potassic composition such as leucititic tephrites, phonolites and trachytes (Santacroce, 1987; Barberi et al. 1981; Bernasconi et al. 1981; Santacroce et al. 2008). Geophysical and borehole data indicate that volcanic activity of SV is subsequent to the emplacement of the Campanian Ignimbrite eruption products (occurred at 39.8 ka; Giaccio et al., 2017), which represents the major Plinian eruption of the nearby Campi Flegrei volcano recorded in the Campanian Plain. The present shape of SV is characterized by a younger cone (Gran Cono) localized within an about E-W oriented elliptical caldera, constrained to the N by an arc-shaped scarp cutting the old Somma Volcano. . The SV multistage summit caldera (located between ca. 560 and 870 m a.s.l.), is the result of caldera collapses (with different geometries) which accompanied the four major Plinian eruptions (Cioni et al., 1999). The oldest Plinian eruption occurred at the SV volcano (i.e. the 18 ka BP Pomici di Base eruption) produced a caldera collapse which truncated the early Somma Volcano, whose crater center was located between the present Gran Cono and the Mt. Somma scarp (Fig.1). Subsequently the last Plinian eruption at SV, occurred in 79 AD, the Gran Cono started to grow discontinuously, with its present shape and structure resulting mostly from the 1631-1944 AD eruptive activity. The oldest outcropping products of the SV volcano are exposed at the base of the

Mt. Somma scarp and date back to about 30 ka BP; while those belonging to the last cycle of activity (1631-1944 AD) are located on top of the scarp itself (Santacroce and Sbrana 2003). Several dykes crosscut the volcanic succession exposed along the caldera wall (Porreca et al., 2006); most of them are sub-vertical, while others show dip directions both outward and inward with respect to the caldera.

It is widely accepted that the SV volcano is characterized by a well-localized magmatic conduit in depth which has determine the whole volcanic activity including both small-scale effusive events and large-scale explosive eruptions (Santacroce, 1987). Millennia long periods of rest, with a closed conduit condition, preceded the largest eruptions (e.g. Rosi et al. 1993); on the contrary an open conduit setting of the volcano is associated to a continuous moderate activity with small-scale eruptions (e.g. Cioni et al. 2008).

The volcanic evolution after the 79 AD Plinian eruption alternated periods of open conduit condition with semi-persistent mainly effusive activity and periods of closed conduit condition (the latter ones preceding the sub-Plinian eruptions of 472 AD and 1631 AD; Rosi et al. 1993). During periods of open conduit condition (e.g. S. Maria cycle and the period 1631-1944; see Cioni et al. 2008), the volcanic activity was often associated with the formation of eruptive fissures (Bianco et al. 1998, Ventura and Vilardo, 1999), such as those localized southward with a N-S direction (1760 AD) and westward with a WSW-ENE direction (1697-1861 AD) (Fig.1). Major fissures are also localized in the NW and NE flank with NW-SE and NE-SW directions, respectively, but with an older age of ca. 22-19 ka BP (Santacroce, 1987; Bianco et al. 1998; Santacroce and Sbrana 2003).Other minor fissures, hosted in the Gran Cono flanks, ranging in age between 1701 and 1899 AD (Santacroce, 1987; Santacroce and Sbrana, 2003; Acocella et al., 2006; Cioni et al., 2008) and showing N-S, E-W and WNW-ESE trends (Tadini et al., 2017).

3. Structural analysis of the Somma-Vesuvio volcano

3.1 Fractures

The SV rocks host fractures, faults and volcanic dykes. Generally fractures in lava layers appear as high dip-angle cooling joints (Fig. 2a, c), mostly orthogonal to the lava boundary surfaces and forming two orthogonal sets (Fig. 2a). Cooling joints within volcanic dykes form roughly square and hexagonal systems (columnar joints, Fig. 2c), with dip-angles ranging from sub-horizontal to sub-vertical, usually orthogonal to the host rock walls (Fig. 2c). Other fractures, with lengths of several tens of meters, crosscut the Mt. Somma scarp, appearing as radial (Fig. 2d) and tangential (Fig. 2e) respect to the caldera. Radial fractures also occur along the inner crater of the Gran Cono (Fig. 2f). Two *en-echelon* macro-fractures crosscutting the 1929 AD pahoehoe lavas (Fig. 3c) along the eastern rim of the caldera (Fig. 3a-c) are characterized by a N-S direction and a total length of ca. 72 m. The easternmost fracture shows at least 1 m of horizontal displacement, with few centimeters of vertical slip and an angular rotation of the hanging wall (Fig. 3c). The westernmost macro-fracture shows a larger length but a minor opening (lesser than 1 m).

Furthermore, also ash and pyroclastic deposits, exposed in the quarries located along the SV flanks, host fractures, usually forming high dip-angle orthogonal joint sets. These fractures are mainly developed in fine grained deposits (e.g. compact ash layers) and less in coarse grained sediments (e.g. pumice layers).

The orientation analysis of the cooling joints in lavas, indicates an almost uniform radial pattern for the fracture directions, with a slight prevalence of the E-W and NE-SW trends (Fig. 4a). On the other hand the orientation data of fractures, within pyroclastic rocks, reveal the occurrence of three main trends: NE-SW, NW-SE and E-W (Fig. 4b). In order to investigate possible preferred orientations of cooling joints, the area was subdivided in 200x200 m-sized cells. For each cell the main fracture direction and the S_3 eigenvector were calculated and analyzed by means of rose diagram and

129 stereographic projection, respectively, as illustrated in Figure 4. The S_3 eigenvector indicates the
130 extension axis calculated through the Bingham method (Bingham, 1974). Fracture dominant
131 directions were calculated through bipolar rose diagrams characterized by an azimuth interval of 10°.
132 Figure 5a and 5b shows the fracture and S_3 directions, respectively, represented in the map as oriented
133 segments. The rose diagram (Fig. 4c) of the main directions of all of fractures (cooling joints collected
134 in lavas and fractures in pyroclasts), marks the prevalence of E-W, ENE-WSW and NNE-SSW
135 directions. The stereographic projection of all S_3 axes indicates a main cluster with a NNW-SSE
136 direction and a secondary cluster with ENE-WSW direction (Fig. 4d). In order to unravel a possible
137 difference between the strain pattern close and far from the Gran Cono center, the preferred
138 orientations of all the fractures were further analyzed subdividing the area in three concentric circular
139 sectors (Fig. 5a): (i) the inner circle includes all fractures hosted in the Gran Cono; (ii) the second
140 circular sector comprises the Mt. Somma scarp and finally (iii) the external ring includes the remnant
141 fractures. For each area, rose diagrams of the fracture main directions were calculated (Fig. 5e-g).
142 The Gran Cono area (Fig. 5a) show a main E-W direction and secondarily N-S, NE-SW and NW-SE
143 directions. For the second circular area (Fig. 5f) the orientation analysis marks the dominant NNE-
144 SSW and E-W directions whereas for the external sector (Fig. 5g) the main directions are ENE-WSW
145 and WNW-ESE. Further analyses of these structural features were carried out subdividing data in two
146 groups (A and B) according to the age of hosting deposits (< 79 AD and > 79 AD, respectively).
147 Resulting rose diagrams indicate that for group A (Fig. 5h), the main trends are NE-SW, E-W and
148 NW-SE, while for group B (Fig. 5i), in addition to the same trends of group A, also the N-S direction
149 occurs.

150

151 *3.2 Dykes*

152 Volcanic dykes, well-exposed along the Mt. Somma scarp and Gran Cono walls, are characterized by
153 variable length, thickness, orientation and geometry. A total of 100 dykes were measured and mapped

154 (Fig. 6a). The analyzed dykes occur as single (Fig. 3g), parallel (Fig. 3h) or *en-echelon* sets (Fig. 3d-
155 f). Dykes are from sub-vertical to moderately and gently dipping both inside and outside the caldera,
156 somewhere as sills (Fig. 3g). Two *en-echelon* conjugate dyke sets bound an NE-SW striking graben
157 (Fig. 3d). In the western sector of the Gran Cono (Fig. 3h) a main N-S sub-vertical dyke and a parallel
158 minor structure crosscut deposits belonging to the period 1855-1872 AD (Santacroce, 1987). Dyke
159 orientation analysis indicates a dominant NE-SW direction (Fig. 6d); however, by normalizing the
160 data according to the length of the dykes, the NE-SW and NW-SE directions appear to be the main
161 ones (Fig. 6e). In order to unravel the relationship between the directions of the dykes located in the
162 Mt. Somma scarp (Fig. 6), we applied the methods illustrated by Porreca et al. (2006) and Quintà et
163 al. (2015). Assuming that the formation of these dykes is synchronous with the eruptive fissures
164 located on the NW and NE flanks, whose ages are older than the first caldera collapse (18 ka; Cioni
165 et al., 1999), we used the center of the old Somma volcano as bench mark for the radial analysis.
166 α, β and δ angles were calculated, where: (i) α is defined as the angle between dyke location and the
167 North (from 0° to 360°); (ii) β is the strike of the dyke (from 0° to 180°) and (iii) δ is the absolute
168 value of the difference between α and β. The δ angle, ranging between 0 and 90°, allows to classify
169 the dykes in i) radial ($\delta \leq 30°$); ii) oblique ($30° \leq \delta \leq 60°$) and iii) tangential ($\delta \geq 60°$). It results that 59%
170 of dykes are radial, 24% oblique and only 17% tangential (Fig. 6c). The α-β contour diagram shows
171 both the main NE-SW trend and the radial pattern (Fig. 6b).

172

173 *3.3 Faults*

174 Most of the faults were observed along the Mt. Somma scarp. The cooling joints in the lava strata,
175 oriented parallel to the caldera scarp (tangential joints) generally show slicken-side steps and
176 striations (Fig. 2a): The latter are characterized by high values of pitch on the tangential planes
177 indicating a dominant normal kinematics whereas, locally on the radial planes, oblique kinematics

178 with pitch angles >45° occurs (Fig. 2a). The larger structures are tens of meters long high-angle
179 normal faults parallel to the caldera scarp showing displacements of few meters (Fig. 7b, c). Rare
180 low-angle faults also occur, whose normal kinematic component is inferred by dislocated planar
181 features such as preexisting dykes (Fig. 2d). These low-angle normal faults are generally crosscut by
182 sub-vertical radial fractures and faults (Fig. 2d). Moreover, low-angle normal faults show few
183 centimeter-sized thick damage zones, marked by a high fracture density (Fig 7a). With respect to the
184 pyroclastic sediments located along the SV flanks, they host few normal faults showing a syn-
185 sedimentary character, such as growing strata and plastic deformation in the hanging wall (Fig. 7e).
186 Slicken-side striations are very rare, locally they occur in scoria deposits always showing dip-slip
187 normal kinematics (Fig. 7d).

188 The stereographic projections of fault poles and the rose diagram of fault directions indicate a
189 dominant E-W direction (Fig. 8a). The rose diagram of the fault main directions, including both faults
190 in lavas and pyroclastic rocks, each one calculated for every cell, shows main E-W and N-S directions
191 and secondary NE-SW and NW-SE directions (Fig. 8b). By means of the P-B-T method (Angelier
192 and Mechler, 1977; Reiter and Acs, 1996–2003) we calculated the T-axes (extension) characterized
193 by NNE-SSW and NNW-SSE directions. Finally the maps of figures 5c and 5d show the fault main
194 directions and the T-axis directions, respectively.

195

196 4. Lineament analysis

197 With the aim to highlight possible connections between the volcano-tectonic activity and the
198 morphologic surface of the SV, lineament extraction has been obtained from the SV Digital Terrain
199 Model (DTM). Lineament analysis on DTMs was previously provided by different authors, with the
200 aim to study volcano-tectonic (Ventura et al., 1999) or geomorphological (Ventura et al., 2005;
201 Alessio et al., 2013) features. In this study we used a DTM with a higher ground resolution (1x1 m)

202 with respect the previous analyses. Elevation data of the SV topography have derived from two
203 different sources: i) the "Ufficio Sistema Informativo Territoriale (SIT)" of the "Provincia di Napoli"
204 (Project "Centro Satellitare Cave della Provincia di Napoli – Ce.CO.SCA"); ii) the "Ministero
205 dell'Ambiente e della Tutela del Territorio e del Mare (MATTM)" with license Creative Commons
206 3.0 Italy (CC BY-SA-3.0IT). These models were provided in 5451 ASCII files (3615 from 2009 flight
207 and 1836 from 2012 flight), matrices of 500 rows x 500 columns having a cell size of 1 meter and
208 geocoded into WGS84 UTM ZONE 33 reference coordinate system. The elevation data of the
209 MATTM instead were acquired during ALS flights occurred in 2008 year. Also this data were
210 provided in matrices with cell sizes of 1 m.
211 With the term "lineament" we mean here any natural linear pattern visible by the shaded reliefs of
212 the study area. Lineaments that clearly represent anthropic features (road cuts, terraces, buildings,
213 etc.; Fig. 9a) or irregularities in the DTM (due to acquisition errors), have been not included in this
214 investigation. For a correct collection of natural lineament data we have selected an area of ca. 71
215 km^2 characterized by more smooth topography and weak urbanization. The investigation scale was
216 defined to 1:10,000. To extract natural lineaments two steps have been performed. For the first step,
217 all the clearly evident natural lineaments have been traced starting from 4 shaded reliefs obtained
218 illuminating the DTM with six different settings of azimuth from N (0°, 45°, 135°, 180°, 225° and
219 315°) and maintaining constant the illumination angle of 45°. As regards the second step, in order to
220 magnify possible directional trends, three different gradient filters (N, NE and NW) have been applied
221 to all the shaded reliefs (in order to enhance the visibility of the features with directions opposite to
222 that of filter itself) combining a directional 3x3 convolution kernel to each matrix of the shaded
223 reliefs. Following the two steps described above, a database of 4095 natural lineaments was
224 implemented (Fig. 9b). Each lineament has been analyzed from the point of views of its (i) length
225 (expressed in meters); (ii) azimuths (expressed in degrees with respect to N) and (iii) spatial locations.
226 Furthermore the (iv) orientation analysis with respect the volcano center was calculated as well. The
227 analysis method is the same of that previously used for the dykes. Assuming that the lineaments are

mostly related to the recent activity of the SV volcano, the Gran Cono center was selected for this analysis. In order to analyze the relationship between lineament orientations and distance from the Gran Cone center, six different circular areas have been identified with radii ranging between 0-1, 0.5-1.5, 1-2, 1.5-2.5, 2-3 and 3-4 km (Fig. 10). We identified more circular areas with respect the fracture orientation analysis, because of the large amount of data uniformly distributed in the study area.

The α-β contour plots (Fig. 10) show that in each pattern, a superposition between radial and regional configurations occur, the latter marked by lineament clustering characterized by N20-30E and N70-80E directions (β), especially for radii lesser than 2.5 km (comprising the Mt. Somma scarp). The two regional directions (about NNE-SSW and ENE-WSW) are well-marked in the rose-diagrams associated to each circular area (Fig. 10). Finally, δ-frequency histograms (Fig. 10) confirm that the most part of lineaments are radial, followed by oblique and only a secondarily tangential.

5. Discussion

The analyzed fractures can be grouped in three main types: i) decimeter-sized cooling joints hosted in lavas, sills and dykes; ii) meter to tens of meters in length tangential/radial fractures, crosscutting different lava layers, scoriae and pyroclastic products; iii) N-S macro-fractures located to the eastern rim of the Mt. Somma scarp, crosscutting the 1929 AD pahoehoe lavas.

The orientation analysis on the whole dataset of the cooling joints, reveals a random direction pattern, on the contrary when analyzed for each 200x200 m cell, preferred orientations result. These fracture preferred azimuths show dominant N-S, E-W, NE-SW and NW-SE directions. Furthermore, the orientation analysis, performed for circular areas centered in the Vesuvio crater, and including all fractures (both in lavas and in pyroclasts) indicates that the N-S and E-W fracture sets are mostly developed close to the Gran Cono and Mt. Somma scarp (0-2 km of radius), whereas the NE-SW and

NW-SE directions are dominant for the external sector (>2 km). Grouping the fracture data by age of the hosting deposits (group A with ages < 79 AD and group B with ages > 79 AD), results that group A fractures show trends NE-SW, E-W and NW-SE; whereas in younger deposits of group B a further N-S trend is present.

The occurrence of preferred orientations for the cooling joints can be related to (i) a synchronous volcano-tectonic stress field (Hancock and Engelder, 1989) or ii) an articulated topography modelled by preferentially oriented volcano-tectonic structures (Fleischmann, 1991). In any case these features suggest that cooling joint pattern is controlled by a preexisting or simultaneous volcano-tectonic deformation field.

As concerning the radial and tangential fractures, they generally form during the volcanic inflation and they can be reactivated as faults during a deflation stage accompanied by a caldera collapse (e.g. Martì et al., 1994). Finally, the open macro-fractures can be related to the ground instability along the volcano slope. This is validated by the occurrence of tilted hanging walls suggesting that the shallow sub-vertical fracture planes downward pass to listric surfaces, typical of the rotational landslides.

The main result of the dyke orientation analysis, carried out in this study, indicates a dominant radial pattern for these structures in agreement with Porreca et al. (2006). However, when considering the preferred orientations, dykes appear to form two main sets with N115E and N50E directions. These orientations are also similar to those of the two eruptive fissures located, respectively, in the NW sector (strike N128E) and NE sector (strike N48E), whose ages are both comprised between 22 and 19 ka (Santacroce, 1987 and Bianco et al. 1998). Probably this temporal interval corresponds to that of most of the dyke formation, presently exposed along the Mt. Somma scarp. On the other hand, the dykes within the Gran Cono, characterized by N-S direction, are hosted in the 1855-1872 AD rocks (Santacroce, 1987). The simultaneous radial and clustered array (anisotropic radial pattern; Acocella and Neri, 2009) of the dyke direction is characteristic of several other volcanoes around the world

such as Etna (Acocella and Neri, 2003) and Stromboli (Tibaldi 2003) in Italy, Fuji in Japan (Takada et al., 2007) and Erta Ale in Ethiopia (Acocella, 2006).

The geometry of the dykes is generally planar, though several dykes located in the Mt. Somma depict a conjugate *en-echelon* array. This geometry suggests that the magma flow within the *en-echelon* apophyses was sub-horizontal, such as stated by Porreca et al. (2006) by means of the Anisotropy Magnetic Susceptibility study. Probably magma flowed within weakness bands bounding a graben structure suggesting a shear component with a normal kinematics for the emplacement of the *en-echelon* dykes. The NE-SW direction of both dominant dyke swarm and *en-echelon* dyke graben, suggest a main extension characterized by a NW-SE direction, at least during their emplacement (22-19 ka BP).

According to Porreca et al. (2006), this configuration occurred with an open volcanic conduit stage (Fig. 11a). On the contrary the closed conduit condition increases the magma pressure triggering the volcano inflation and the prevalence of the radial field with the formation of both radial and tangential fractures (Fig. 11b).

Such as observed in several volcanic settings (e.g. Acocella, 2007 and references therein), the development of ring faults is related to caldera collapse processes. At SV, these structures crosscut the whole volcanic sequence; however, they worked at the meso-scale, reactivating preexisting planes including cooling joints. All the slicken-side striations observed on the tangential planes indicates a normal dip-slip kinematics, whereas the radial faults show an oblique kinematics. We conclude that during caldera collapse stages, tangential and radial fractures previously formed as result of the volcanic inflation or as cooling joints, reactivate as (i) normal ring faults inward dipping to the caldera and (ii) transfer faults, respectively (Fig. 11c). In this case transfer faults have allowed that different blocks independently move toward the center of the collapsing caldera.

299 Another type of structure is represented by low-angle normal faults. Despite their length, they show
300 small displacements, crosscutting dykes and in turn cut by radial fractures and ring faults. Probably
301 low-angle normal faults are related to the inflation stage that triggered gravitational instabilities along
302 the volcano flanks (Fig. 11b).

303 Faults were observed also along the volcano slopes crosscutting pyroclastic deposits. They are
304 frequently associated to plastic deformation features suggesting that they formed synchronously to
305 the eruption, such as occurred in other volcanic settings (e.g. Campi Flegrei; Vitale and Isaia, 2014;
306 Solfatara volcano; Isaia et al., 2015). Faults as a whole show N-S, E-W, NW-SE and NE-SW main
307 directions, and the T-axis indicate a NNE-SSW extension, well-fitting with kinematic analysis carried
308 out on faults by Bianco et al. (1998).

309 At this point, some considerations have to be done about the relationship between faults, caldera and
310 vent main centers and eruptive fissures. The SV eruptive history was characterized by an alternation
311 of open and closed conduit stages with four caldera collapses (Cioni et al., 1999). However, the
312 caldera and vent main centers were localized in different sectors of the present caldera depicting a
313 triangular area bounded by ca. E-W, N-S and NE-SW sides (Fig. 1). The (i) caldera centers of Mercato
314 (8 ka; Cioni et al. 2008) and Pompeii (79 AD) eruptions; the (ii) vent centers of Mt. Somma volcano
315 and the recent Gran Cono; (iii) the eruptive fissures located in the southern flank of SV and the (iv)
316 dykes within the Gran Cono, are all aligned along a N-S lineament. The N-S and E-W directions are
317 well-marked in the fracture preferred directions located close to the Gran Cono and also by the rose
318 diagram of eruptive fissures (Tadini et al., 2017). All these features suggest that the SV conduit is
319 localized in the area between the intersections of major faults characterized by the well-known
320 Apenninic (NW-SE) and anti-Apenninic (NE-SW) trends and probably by a major N-S fault.

321 Finally, the lineament analysis carried out on a high-resolution DTM, marks a superposition of (i) a
322 clustered pattern, characterized by NNE-SSW and ENE-WSW directions, and (ii) a radial pattern.
323 However, the clear separation between these two configurations, suggest that they were recorded in

different stages (e.g. Quintà et al., 2015). As discussed before, the radial pattern is the expression of a closed conduit during a volcano inflation with eventually a subsequent caldera collapse (Fig. 11b, c); on the contrary a clustered pattern could be related to an open conduit (Fig. 11a) characterized by a prevailing unidirectional extension and a very weak radial stress field. In the case of a closed conduit the volcanic stress field (marked by radial pattern) overcome the regional stress field (marked by a clustered pattern).

6. Conclusions

This study provides a general framework of deformation at meso-scale of Somma Vesuvio volcano. Different kinds of fractures and faults were observed and measured. Cooling joints occur in lava layers and dykes; metric fractures crosscutting several volcanic deposits generally occur as radial and tangential with respect to the caldera/cone center. Macro-fractures, locally present in the eastern SV flank, are related to rotational landslides. Cooling joints, oriented parallel and orthogonal to the Mt. Somma scarp, were reactivated as normal and oblique faults, respectively. Metric to decametric high-angle normal ring faults bound the caldera rim showing few meters of displacement. Sporadic decametric low-angle normal faults are located in Mt. Somma scarp crosscutting early dykes, in turn deformed by radial and tangential fractures and ring faults. Finally, centimetric, syn-eruptive normal faults occur in pyroclastic deposits located along the SV flanks.

Dykes occur as single structures or sets with parallel or *en-echelon* geometries. Generally, the latter structures are located at the boundaries of structural depression, suggesting a synchronous normal shear component during their development. Orientation analyses highlighted a clustered arrangement for all of the studied structures when analyzed with respect to their spatial location (this latter performed by subdividing the area in cells and in circular areas) or grouped in two temporal classes (older or younger than 79 AD). Results indicate that there are four dominant directions (NW-SE, NE-

SW, N-S and E-W). The well-known Apenninic (NW-SE) and anti-Apenninic (NE-SW) trends are prevalent for structures located in older rocks (<79 AD) and in sectors far from the Gran Cono (>2 km), while N-S and E-W directions are better recorded in younger rocks mainly localized close to the Gran Cono.

The orientation of the dykes and morphological lineaments (the latter ones extracted from DTM) were studied with respect to the old Somma volcano and Gran Cono centers, respectively. These analyses mark a superposition between radial and clustered strain patterns. We envisage that these two dominant patterns are related to different volcanic evolution stages: during a closed conduit, the volcanic inflation forms a uniform strain field, related to the stress localization above the magma chamber center, largely exceeding unidirectional regional strain fields. On the other hand during the open conduit activity, the intensity of radial pattern is very low and the regional strain pattern prevails. In the first case, the volcano inflation produces tangential and radial fractures that, in a possible subsequent caldera collapse stage, can be reactivated as normal and oblique faults, respectively, the latter acting as transfer structures. In the second case, the occurrence of an open conduit allows the development of dykes with horizontal magma flows and eruptive fissures often forming *en-echelon* sets.

References

Acocella V, Neri M (2009) Dike propagation in volcanic edifices: Overview and possible developments. Tectonophysics 471:67–77.

Acocella V. (2007) Understanding caldera structure and development: An overview of analogue models compared to natural calderas. Earth Science Reviews 85:125–160.

Acocella V (2006) Regional and local tectonics at Erta Ale caldera, Afar (Ethiopia). J Struct Geol 28:1808–1820

Acocella V, Porreca M, Neri M, Mattei M, Funiciello R (2006) Fissure eruptions at Mount Vesuvius (Italy): insights on the shallow propagation of dikes at volcanoes. Geology 34:673–676.

Acocella V, Neri M (2003) What makes flank eruptions? The 2001 Etna eruption and its possible triggering mechanisms. Bull Volcanol 65:517–529.

Alessio G, De Falco M, Di Crescenzo G, Nappi R, Santo A (2013) Flood hazard of the Somma-Vesuvius region based on historical (19-20th century) and geomorphological data. Annals of Geophysics, 56:S0434.

Angelier J, Mechler P (1977) Sur une méthode graphique de recherche des contraintes principales égalment utilisable en tectonique et en seismologie: La méthode des dièdres droits. B Soc Geol Fr 19:1309–1318.

Barberi F, Bizouard H, Clocchiatti R, Metrich N, Santacroce R, Sbrana A (1981) The Somma–Vesuvius magma chamber: a petrological and volcanological approach. Bull Volcanol 44: 295–315.

Becerril L, Galindo I, Martí J, Gudmundsson A (2015). Three-armed rifts or masked radial pattern of eruptive fissures? The intriguing case of El Hierro volcano (Canary Islands). Tectonophysics, 647–648:33–47.

387 Bernasconi A, Bruni P, Gorla L, Principe C, Sbrana A (1981) Risultati preliminari dell'esplorazione
388 geotermica profonda nell'area vulcanica del Somma-Vesuvio. Rend Soc Geol lt 4:237-240.

389 Bianco F, Castellano M, Milano G, Ventura G, Vilardo G (1998) The Somma–Vesuvius stress field
390 induced by regional tectonics: evidences from seismological and mesostructural data. Journal
391 of Volcanology and Geothermal Research 82:199-218.

392 Bingham C (1974) An antipodally symmetric distribution on the sphere. Annals of Statistics 2:1201–
393 1225.

394 Borgia A, Tizzani P, Solaro G, Manzo M, Casu F, Luongo G, Pepe A, Berardino P, Fornaro G,
395 Sansosti E, Ricciardi GP, Fusi N, Di Donna G, Lanari R (2005) Volcanic spreading of
396 Vesuvius, a new paradigm for interpreting its volcanic activity. Geophysical Research Letters
397 32:l03303.

398 Brancaccio L, Cinque A, Romano P, Rosskopf C, Russo F, Santangelo N, Santo A, (1991)
399 Geomorphology and neotectonic evolution of a sector of the Tyrrhenian flank of the Southern
400 Apennines (region of Naples, Italy), Z Geomorphol 82:47–58.

401 Brocchini D, Principe C, Castradori D, Laurenzi MA, Gorla L (2001) Quaternary evolution of the
402 southern sector of the Campania Plain and early Somma-Vesuvius activity: Insights from the
403 Trecase 1 well. Mineral Petrol 73:67–91.

404 Cinque A, Alinaghi HH, Laureti L, Russo F (1987) Osservazioni preliminari sull'evoluzione
405 Geomorfologica della Piana Del Sarno (Campania, Appennino Meridionale). Geogr Fis
406 Dinam Quat 10:161-174.

407 Cioni R, Santacroce R, Sbrana A (1999) Pyroclastic deposits as a guide for reconstructing the multi-
408 stage evolution of the Somma-Vesuvius Caldera. Bull Volcanol 60:207–222

409 Cioni R, Bertagnini A, Santacroce R, Andronico D (2008) Explosive activity and eruption scenarios
410 at Somma-Vesuvius (Italy): Towards a new classification scheme. Journal of Volcanology
411 and Geothermal Research 178:331-346.

412 D'Auria L, Massa B, De Matteo A (2014) The stress field beneath a quiescent stratovolcano: The
413 case of Mount Vesuvius. J Geophys Res Solid Earth 119:1181–1199.

414 de Gennaro M, Calcaterra D, Langella A (2013) Le Pietre storiche della Campania: dall'oblio alla
415 riscoperta. p. 329-342, Napoli: Luciano Editore, ISBN: 9788860261823.

416 De Natale G, Kuznetzov I, Kronrod T, Peresan A, Sarao A, Troise C, Panza GF (2004) Three decades
417 of seismic activity at Mt. Vesuvius: 1972-2000. Pure Appl Geophys, 161:123-144.

418 Di Stefano R, Chiarabba C (2002) Active source tomography at Mt. Vesuvius: Constraints for the
419 magmatic system. Journal of Geophysical Research 107.

420 Fleischmann KH (1991) Interaction between jointing and topography: a case study at Mt Ascutney,
421 Vermont, U.S.A. Journal of Structural Geology 13:357-361.

422 Giaccio B, Hajdas I, Isaia R, Deino A, Nomade S (2017) High-Precision 14C and 40Ar/39Ar Dating
423 of the Campanian Ignimbrite (Y-5) Reconciles the Time-Scales of Climatic-Cultural
424 Processes at 40 Ka. Sci Rep 7:45940.

425 Gudmundsson A (1995) Infrastructure and mechanics of volcanic systems in Iceland. Journal of
426 Volcanology and Geothermal Research 64:1-22.

427 Gudmundsson A (2006) How local stresses control magma-chamber ruptures, dyke injections, and
428 eruptions in composite volcanoes. Earth Sci Rev 79:1–31.

429 Hancock PL, Engelder T (1989) Neotectonic joints. GSA Bull 101:1197– 1208.

430 Isaia R, Vitale S, Di Giuseppe MG, Iannuzzi E, Tramparulo FD'A, Troiano A (2015) Stratigraphy,
431 structure and volcano-tectonic evolution of Solfatara maar-diatreme (Campi Flegrei, Italy).
432 GSA Bull 127:1485–1504.

433 ISPRA, 2017 Carta Geologica d'Italia alla scala 1:50.000, foglio 448 "Ercolano".
434 http://www.isprambiente.gov.it/Media/carg/448_ERCOLANO/Foglio.html

435 Marinoni L, Gudmundsson A (2000) Dykes, faults and palaeostresses in the Teno and Anaga massifs
436 of Tenerife (Canary Islands). Journal of Volcanology and Geothermal Research 103:83-103

437 Martì J, Ablay GJ, Redshaw LT, Sparks RSJ (1994). Experimental studies of collapse calderas. J
438 Geol Soc London 151:919–930.

439 Marturano A, Aiello G, Barra D, Fedele L, Grifa C, Morra V, Berg R, Varone A (2009) Evidence for
440 Holocenic uplift at Somma-Vesuvius. Journal of Volcanology and Geothermal Research
441 184:451–461.

442 McGuire WJ, Pullen AD (1989) Location and orientation of eruptive fissures and feeder-dykes at
443 Mount Etna: influence of gravitational and regional stress regimes. Journal of Volcanology
444 and Geothermal Research 38:325–344.

445 Muller OH, Pollard DD (1977) The stress state near Spanish Peaks, Colorado, determined from a dike
446 pattern. Pure Appl Geophys 115:69–86.

447 Nakamura K (1977) Volcanoes as possible indicators of tectonic stress orientation-principle and
448 proposal. Journal of Volcanology and Geothermal Research 2:1–16.

449 Odé H (1957) Mechanical analysis of the dike pattern of the Spanish Peaks area, Colorado. GSA
450 Bulletin 68:567-576.

451 Paoletti V, Passaro S, Fedi M, Marino C, Tamburrino S, Ventura G (2016) Sub-circular conduits and
452 dikes offshore the Somma-Vesuvius volcano revealed by magnetic and seismic data.
453 Geophysical Research Letters 43: 9544–9551

454 Pinel V, Jaupart C (2003). Magma chamber behavior beneath a volcanic edifice. Journal of
455 Geophysical Research 108

Pollard DD, Delaney PT, Duffield WA, Endo ET, Okamura AT (1983) Surface deformation in volcanic rift zones. Tectonophysics 94:541-584.

Porreca M, Acocella V, Massimi E, Mattei M, Funiciello R, De Benedetti AA (2006) Geometric and kinematic features of the dike complex at Mt. Somma, Vesuvio (Italy). Earth and Planetary Science Letters 245:389-407.

Quintà A, Tavani S, Roca E (2012) Fracture pattern analysis as a tool for constraining the interaction between regional and diapir-related stress fields: Poza de la Sal Diapir (Basque Pyrenees, Spain). Alsop GI Archer SG, Hartley AJ, Grant NT, Hodgkinson R (eds). Salt Tectonics, Sediments and Prospectivity. Geological Society London Special Publications 363:521–532.

Reiter F, Acs P (1996–2003) TectonicsFP. Software for structural geology. Innsbruck University, Austria

Rosi M, Principe C, Vecci R (1993) The 1631 Vesuvius eruption. A reconstruction based on historical and stratigraphical data. Journal of Volcanology and Geothermal Research 58:151-182

Santacroce R (1987) Somma Vesuvius, C.N.R., Rome, 251.

Santacroce R, Sbrana A (2003) Carta Geologica del Vesuvio, Scala 1:15000, Progetto CARG, Servizio Geologico Nazionale-Consiglio Nazionale delle Ricerche.

Santacroce R, Cioni R, Marianelli P, Sbrana A, Sulpizio R, Zanchetta G, Donahue DJ, Joron JL (2008) Age and whole rock-glass compositions of proximal pyroclastics from the major explosive eruptions of Somma-Vesuvius: a review as a tool for distal tephrostratigraphy. Journal of Volcanology and Geothermal Research 177:1-18.

Santangelo N, Ciampo G, Di Donato V, Esposito P, Petrosino P, Romano P, Russo Ermolli E, Santo A, Toscano F, Villa I (2010) Late Quaternary buried lagoons in the northern Campania plain (southern Italy): evolution of a coastal system under the influence of volcano-tectonics and eustatism Italian Journal of Geosciences. 129:156 – 175.

480 Tadini A, Bevilacqua A, Neri A, Cioni R, Aspinall WP, Bisson M, Isaia R, Mazzarini F, Valentine,
481 GA, Vitale S, Baxter PJ, Bertagnini A, Cerminara M, de Michieli Vitturi M, Di Roberto A,
482 Engwell S, Esposti Ongaro T, Flandoli F, Pistolesi M, 2017. Assessing future vent opening
483 locations at the Somma-Vesuvio volcanic complex: 2. Probability maps of the caldera for a
484 future Plinian/sub-Plinian event with uncertainty quantification: Vent Opening Probability
485 map for Vesuvio. J Geophys Res Solid Earth 122:1-20.

486 Takada A, Ishizuka Y, Nakano S, Yamamoto T, Kobayashi M, Suzuki Y (2007) Characteristic and
487 evolution inferred from eruptive fissures of Fuji volcano, Japan. In: Aramaki S (Ed), Fuji
488 Volcano Volcanol Soc Japan 183–202.

489 Tibaldi A (2003) Influence of cone morphology on dikes, Stromboli, Italy. Journal of Volcanology
490 and Geothermal Research 126:79–95.

491 Ventura G, Vilardo G (1999) Slip tendency analysis of the Vesuvius faults: Implication for the
492 seismotectonic and volcanic hazard assessment. Geophys Res Lett 26:3229–3232.

493 Ventura G, Vilardo G, Bruno PP (1999) The role of flank failure in modifying the shallow plumbing
494 system of volcanoes: an example from Somma-Vesuvius, Italy. Geophysical research letters,
495 26:3681-3684.

496 Ventura G, Vilardo G, Bronzino G, Gabriele G, Nappi R, Terranova C (2005) Geomorphological
497 map of the Somma-Vesuvius volcanic complex (Italy). Journal of Maps 2005:30-37.

498 Vezzoli L, Renzulli A, Menna M (2014) Growth after collapse: the volcanic and magmatic history of
499 the Neostromboli lava cone (island of Stromboli, Italy). Bull Volcanol 76:1-24.

500 Vitale S, Isaia R (2014) Fractures and faults in volcanic rocks (Campi Flegrei, southern Italy): Insight
501 into volcano-tectonic processes: International Journal of Earth Sciences 103:801–819.

502 Zollo A, Marzocchi W, Capuano P, Lomax A, Iannaccone G (2002) Space and time behaviour of
503 seismic activity and Mt. Vesuvius volcano, Southern Italy. Bull Seismol Soc Am 92:625–640.

504 **Figure captions:**

505

506 Fig. 1. Geological map of the Somma-Vesuvio (ISPRA, 2017). Eruptive fissure data from Santacroce,
507 1987 and Bianco et al. 1998. Vent data from Bianco et al., 1998; Paoletti et al., 2016. Fault (literature)
508 data from Bianco et al. 1998. Caldera and major cone rim data from Cioni et al., 1999. Coordinates
509 are expressed in the UTM WGS84 coordinate system.

510

511 Fig. 2. a) Reactivated cooling joint both radial and tangential; b) plumose structure in lavas; c)
512 orthogonal sub-vertical cooling joint sets in dykes; d) radial fractures meter-length and low angle
513 normal faults hosted along Somma Mt. scarp; e) tangential fractures hosted in Mt. Somma products;
514 f) radial fractures hosted in the Gran Cono crater.

515

516 Fig. 3. a) Satellite image of the macro-fractures in the eastern side of the Somma scarp. b-c) pictures
517 of the macro-fracture. d) Panoramic view of en-echelon dykes; e-f) pictures of the dextral and sinistral
518 en-echelon dyke arrays; g) single dyke with complex geometry; h) two parallel dykes hosted in the
519 1855-1872 AD deposits of Vesuvio.

520

521 Fig. 4. Stereographic projections (lower hemisphere, equal-area net), contour plots and rose-diagrams
522 of fractures and S_3 eigenvectors.

523

524 Fig. 5. Maps of a) fracture main directions; b) S3 directions; c) fault main directions and d) T-
525 directions. Rose-diagrams of main directions for fractures included in the e) area 1; f) area 2 and g)
526 area 3. Rose-diagrams of main directions for fractures included in the h) deposits older than 79 AD
527 and i) deposits younger than 79 AD.

528

529 Fig. 6. a) Map of analyzed dykes; b) α (dyke azimuths) vs β diagram (see the text for the explanation);
530 c) histogram of the δ-frequency; d-e) rose diagram of dyke directions.

531

532 Fig. 7. a) Normal fault plane developing a few centimeter-size damage zone; b-c) tens of meters long
533 high-angle normal faults parallel to the caldera scarp; d) normal fault plane showing slicken-side
534 striations in scoriae; e) syn-sedimentary normal fault with growing strata hosted in pyroclastic
535 deposits.

536

537 Fig. 8. Stereographic projections, contour plots and rose-diagrams of faults and T-axes.

538

539 Fig. 9. a) Criteria for lineaments recognition; b) study area and traced lineaments.

540

541 Fig. 10. α (lineament azimuths) vs β diagram (see the text for the explanation), histogram of the δ-
542 frequency and rose diagram of lineament directions calculated for six different circles (centered on
543 the Gran Cono) enclosing areas a) 0-1 km, b) 0.5-1.5 km, c) 1-2 km, d) 1.5-2.5 km, e) 2-3 km and f)
544 3-4 km from the Gran Cono center.

545

546 Fig. 11. Cartoons showing deformation structures formed during: a) opened conduit condition; b)
547 closed conduit condition with volcano inflation; c) closed conduit condition with caldera collapse.

Figure 1

Click here to download Figure Fig. 1.tif

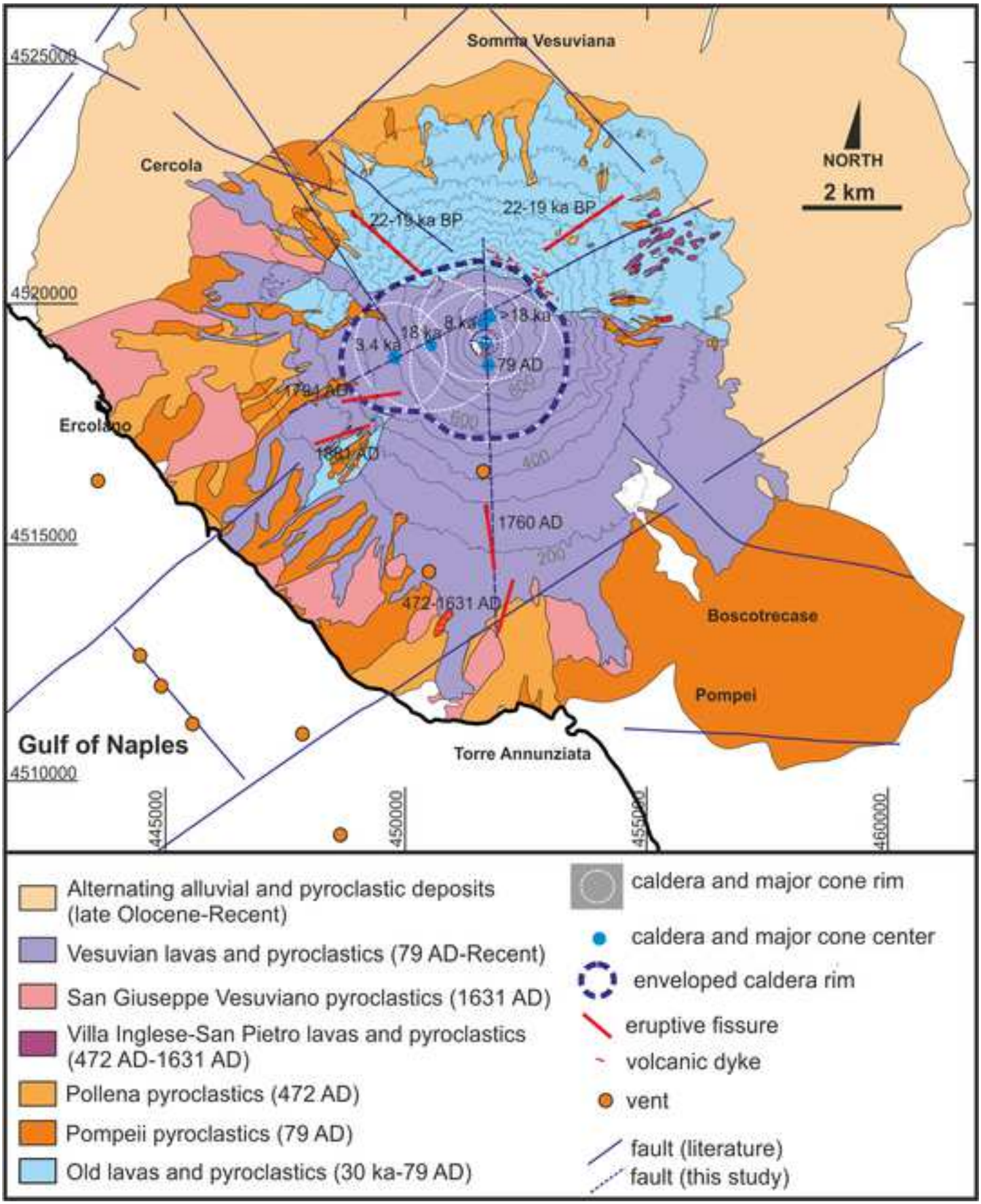

Figure 2

Click here to download Figure Fig. 2.tif

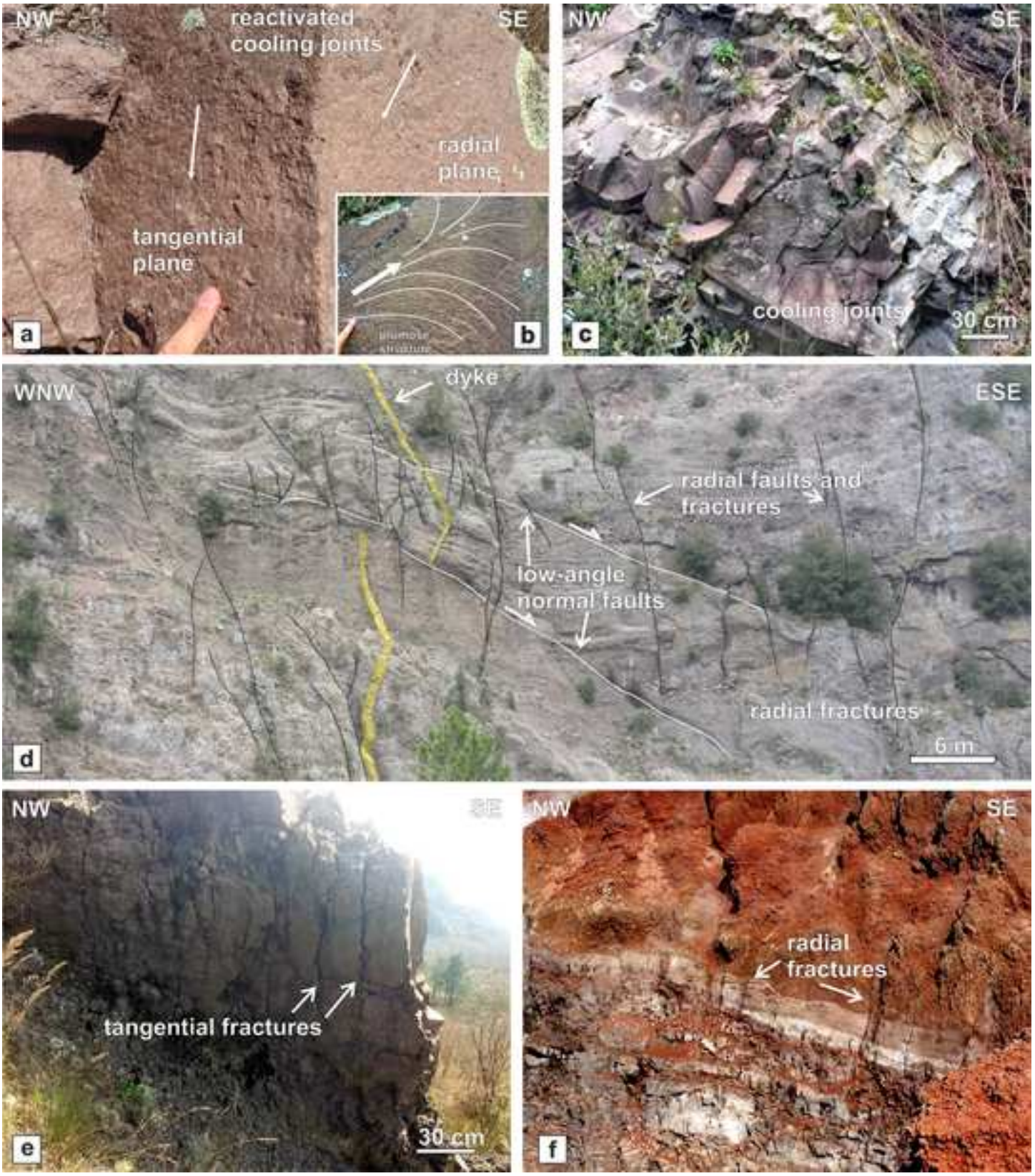

Figure 3

Click here to download Figure Fig. 3.tif

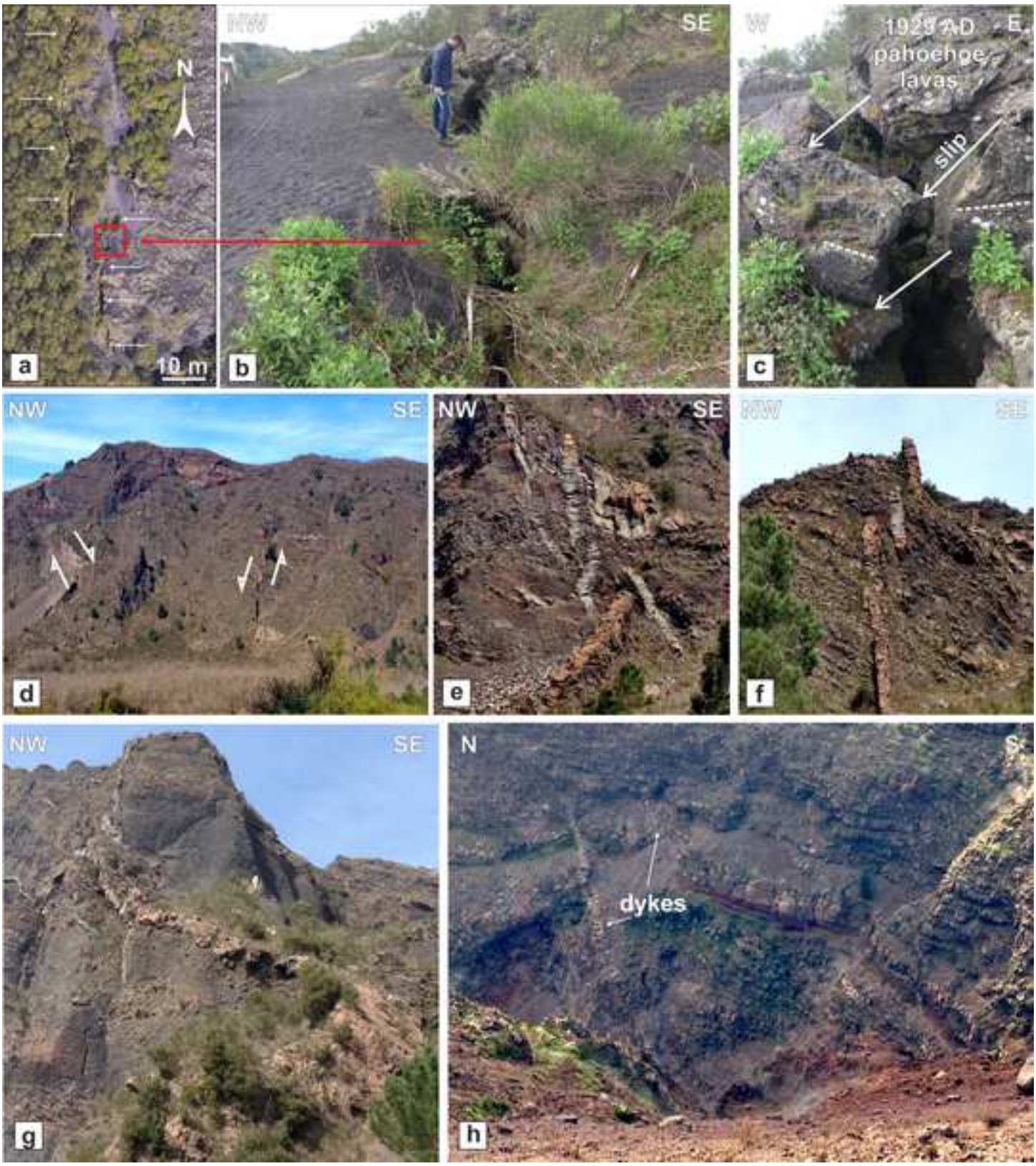

Figure 4

Click here to download Figure Fig. 4.tif

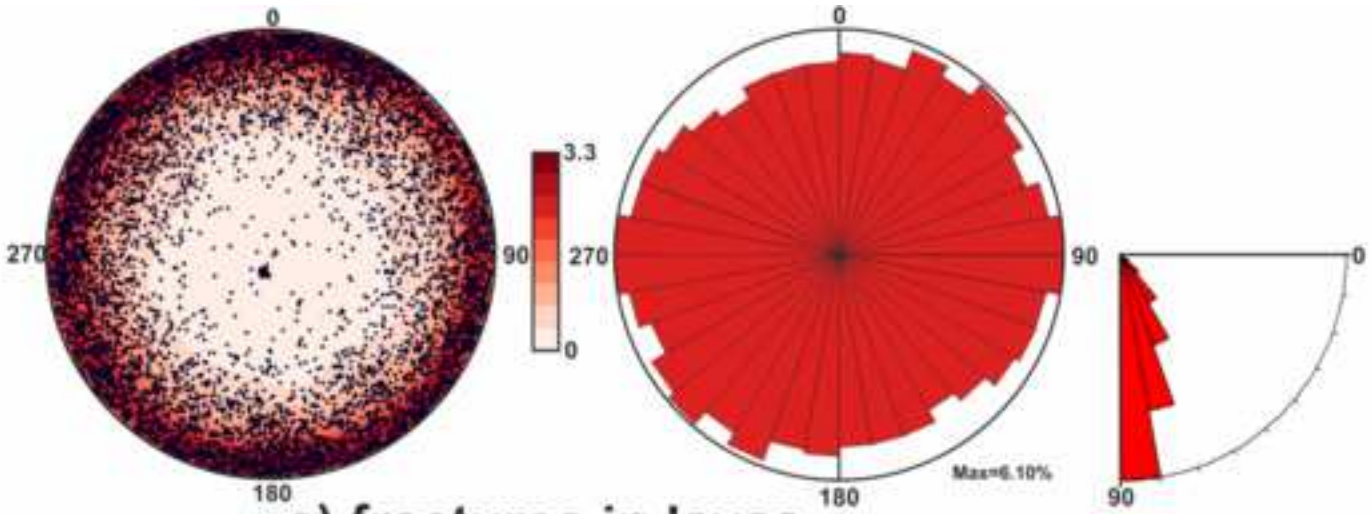

a) fractures in lavas, n= 8320

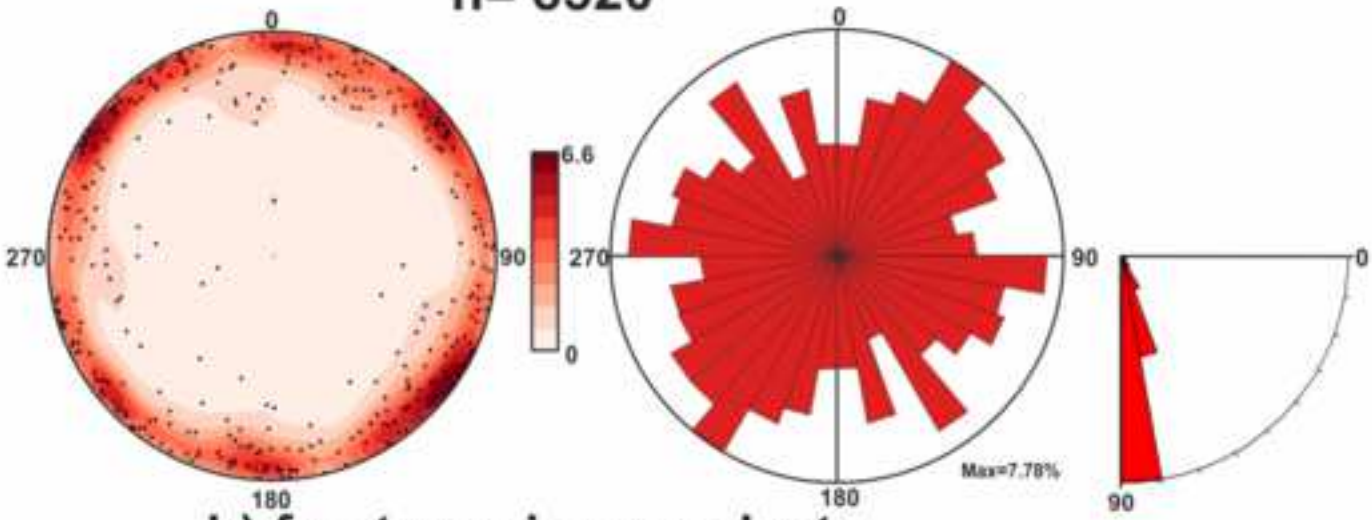

b) fractures in pyroclasts, n= 360

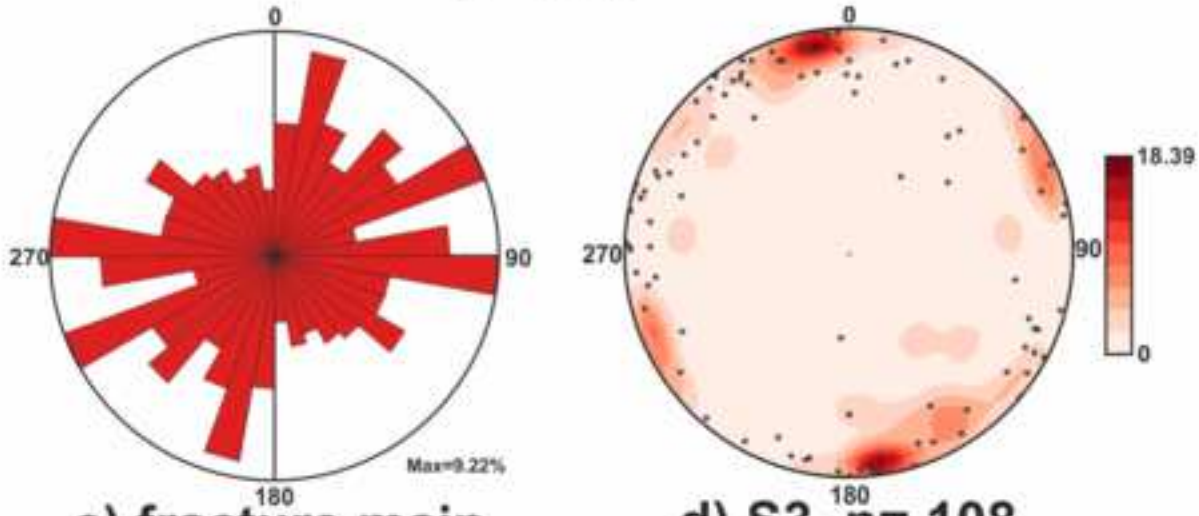

c) fracture main directions, n= 192

d) S3, n= 108

Figure 5

Click here to download Figure Fig. 5.tif

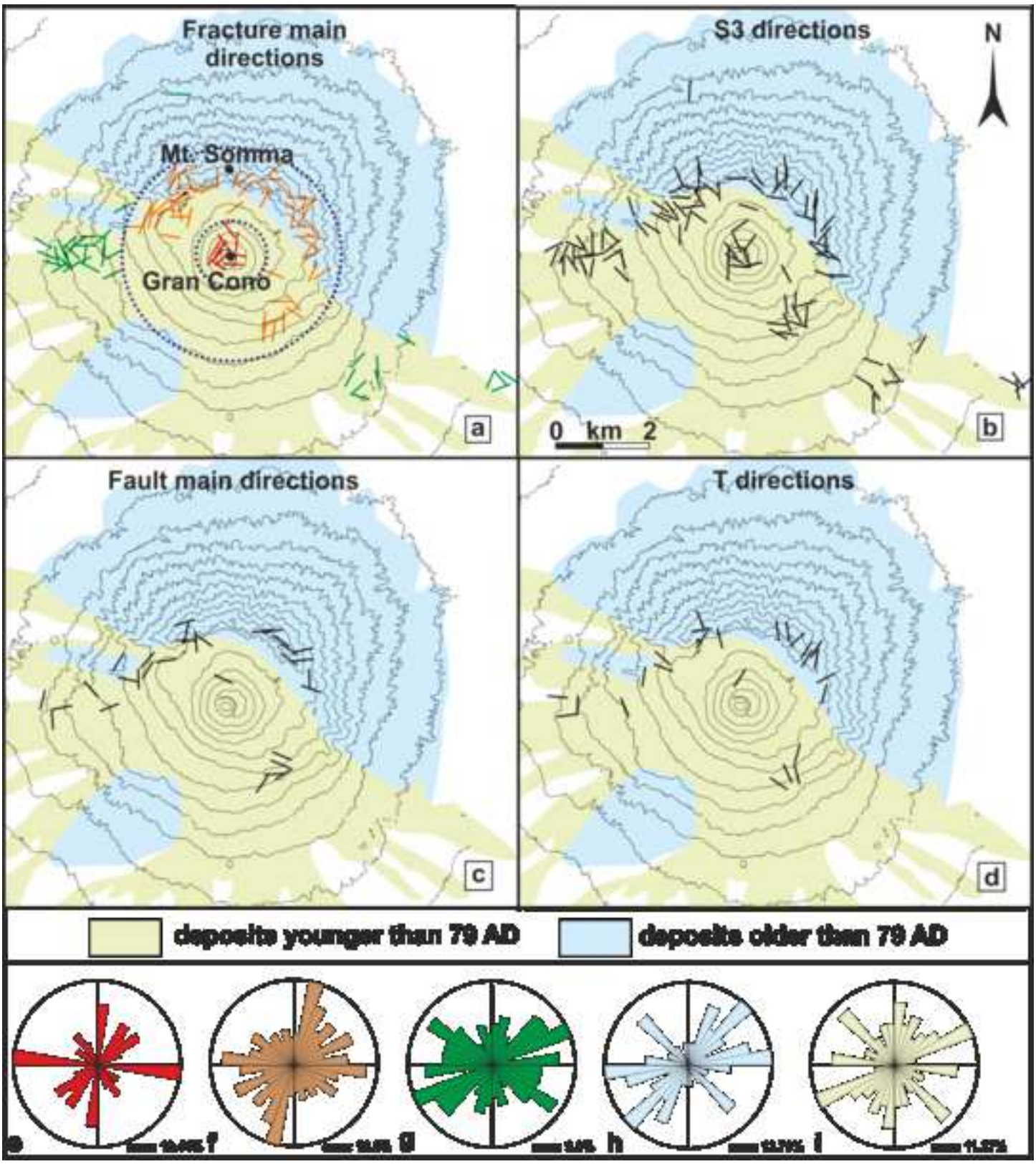

Figure 6

Click here to download Figure Fig. 6.tif

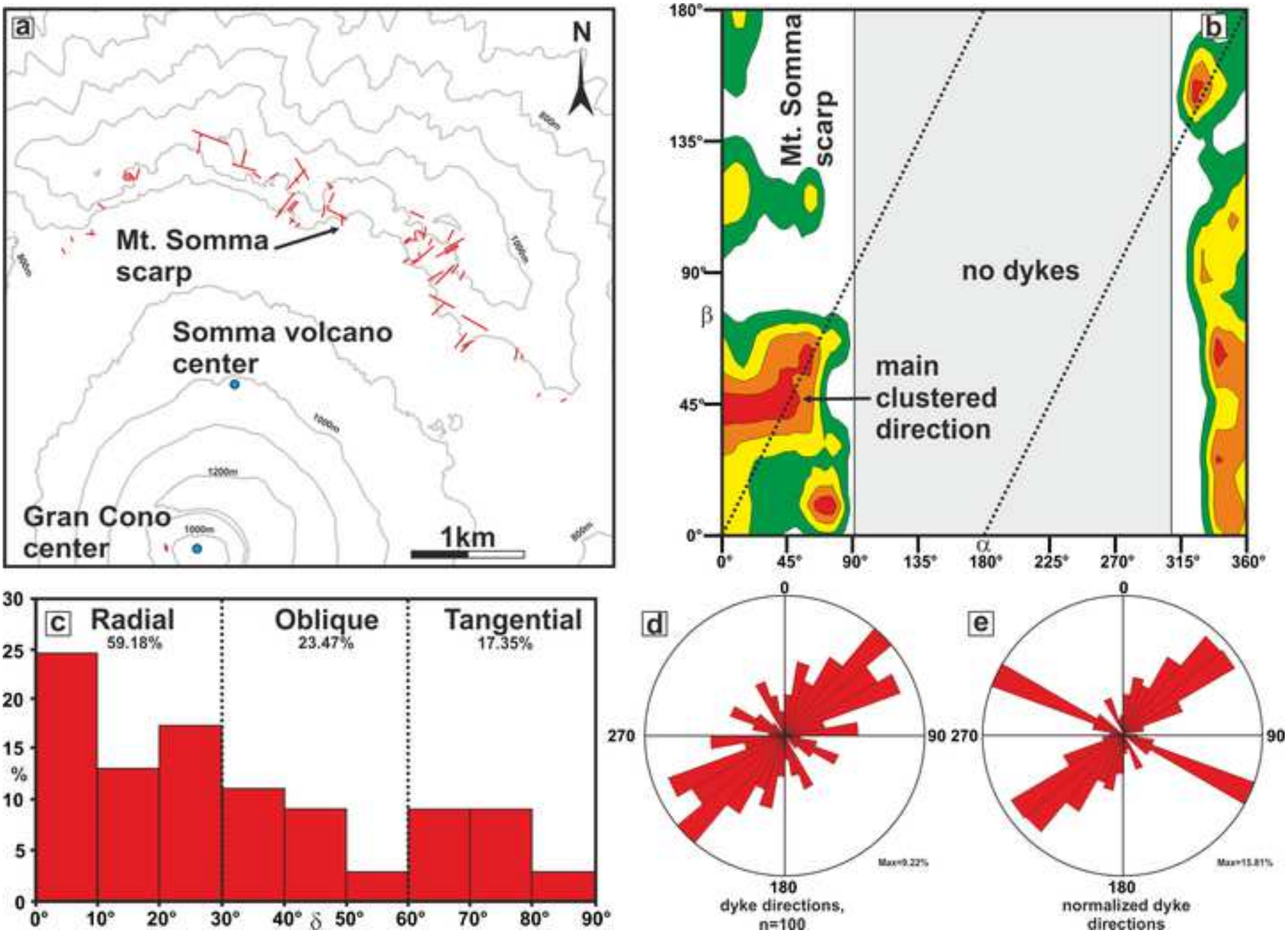

Figure 7

Click here to download Figure Fig. 7.tif

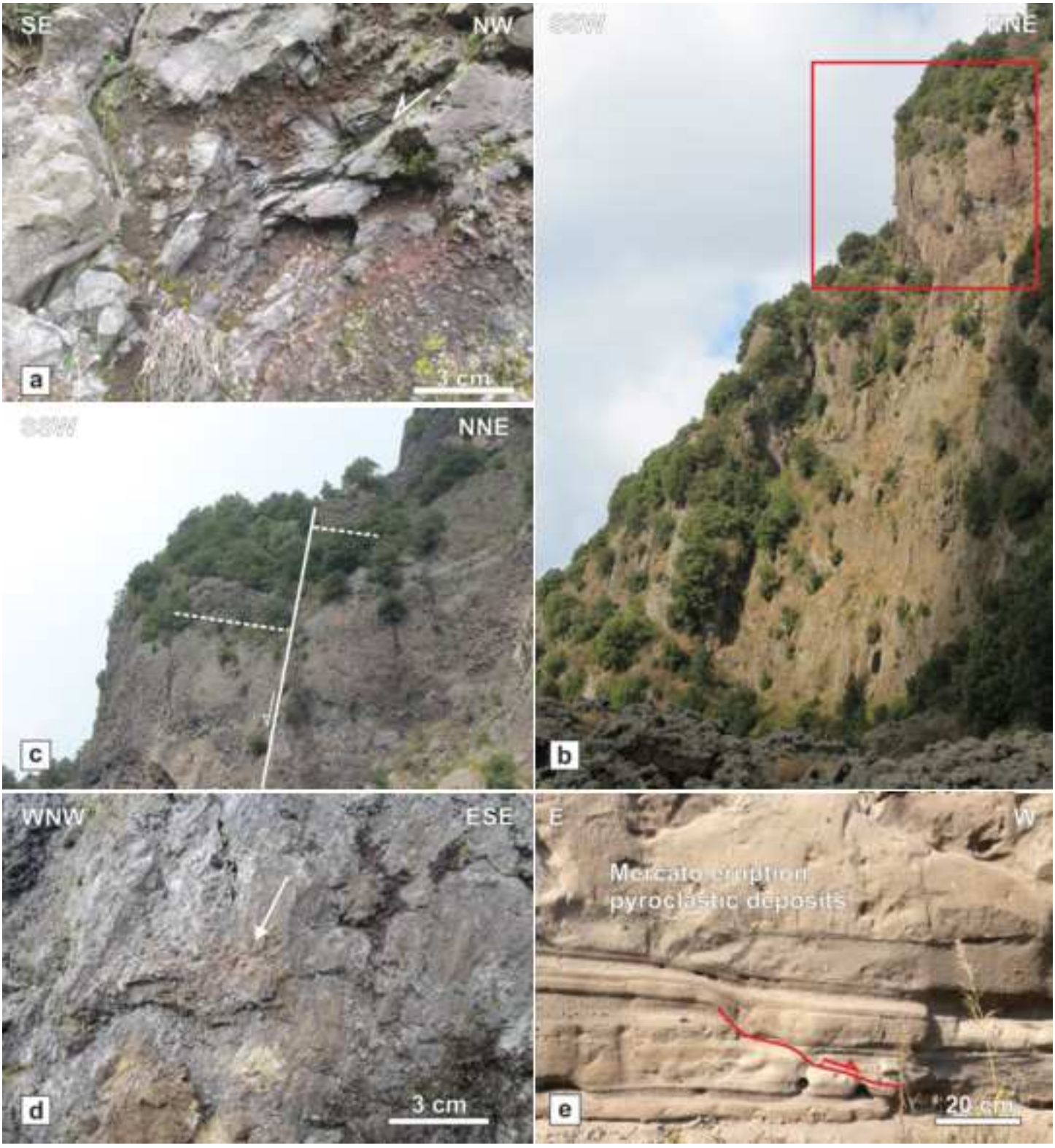

Figure 8

Click here to download Figure Fig. 8.tif

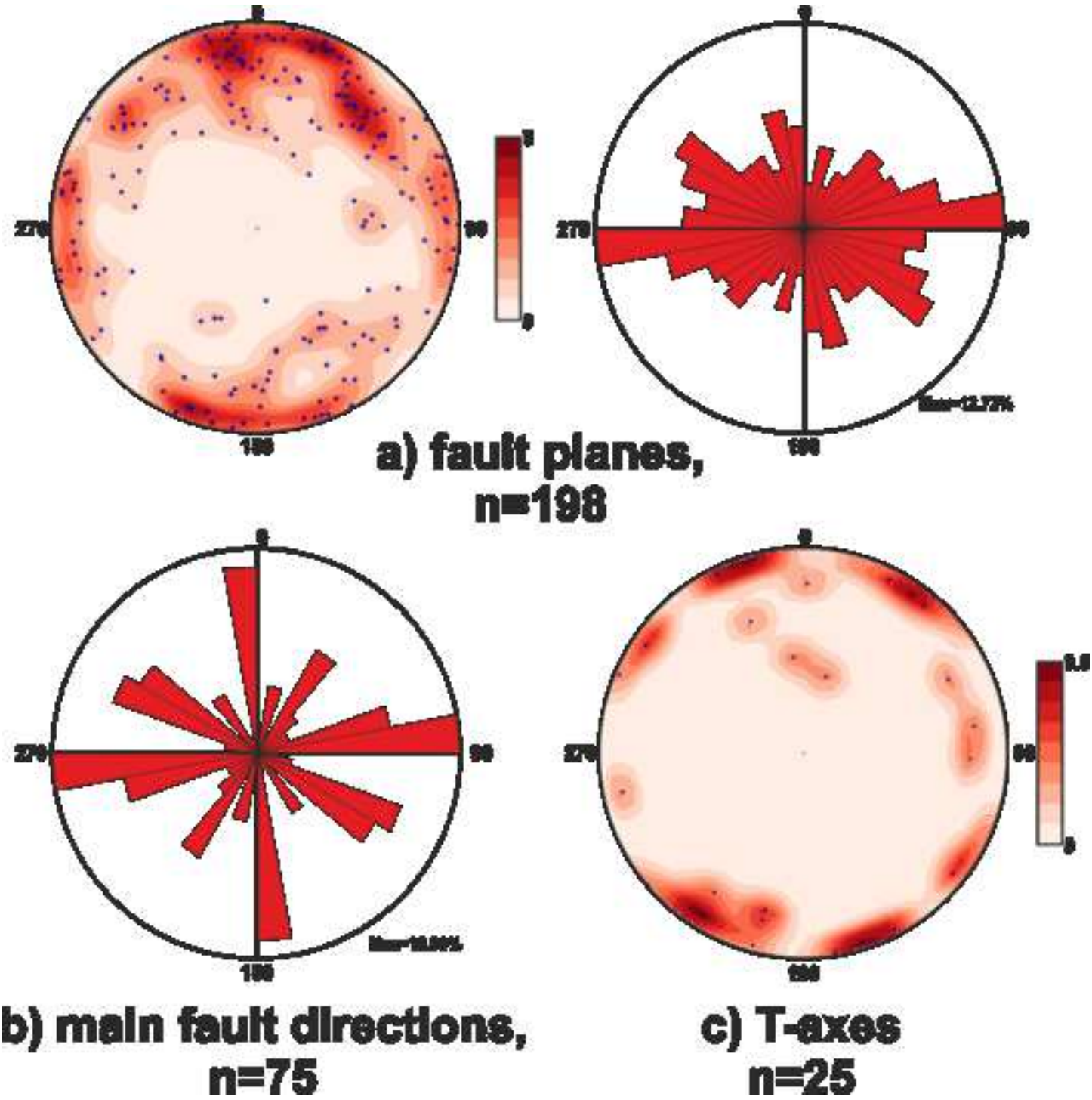

Figure 9

Click here to download Figure Fig. 9.tif

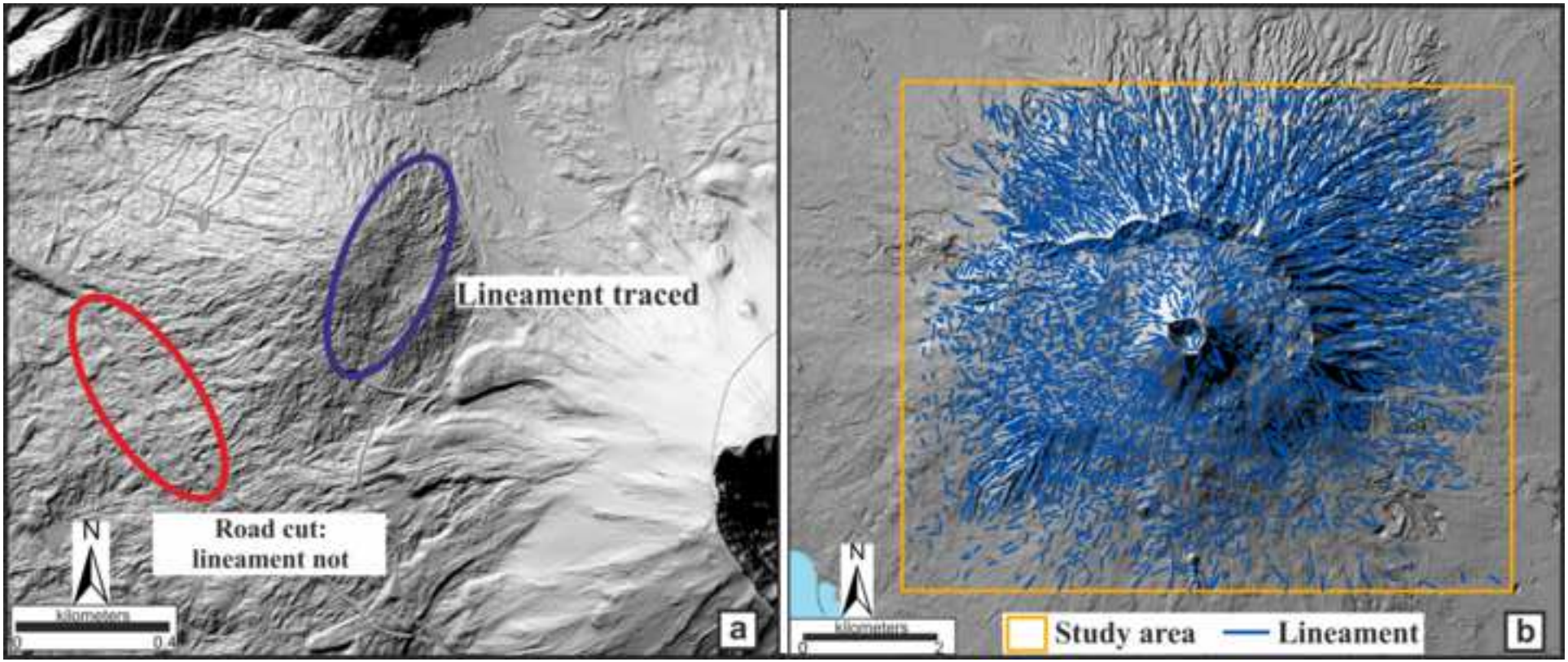

Figure 10

Click here to download Figure Fig. 10.tif

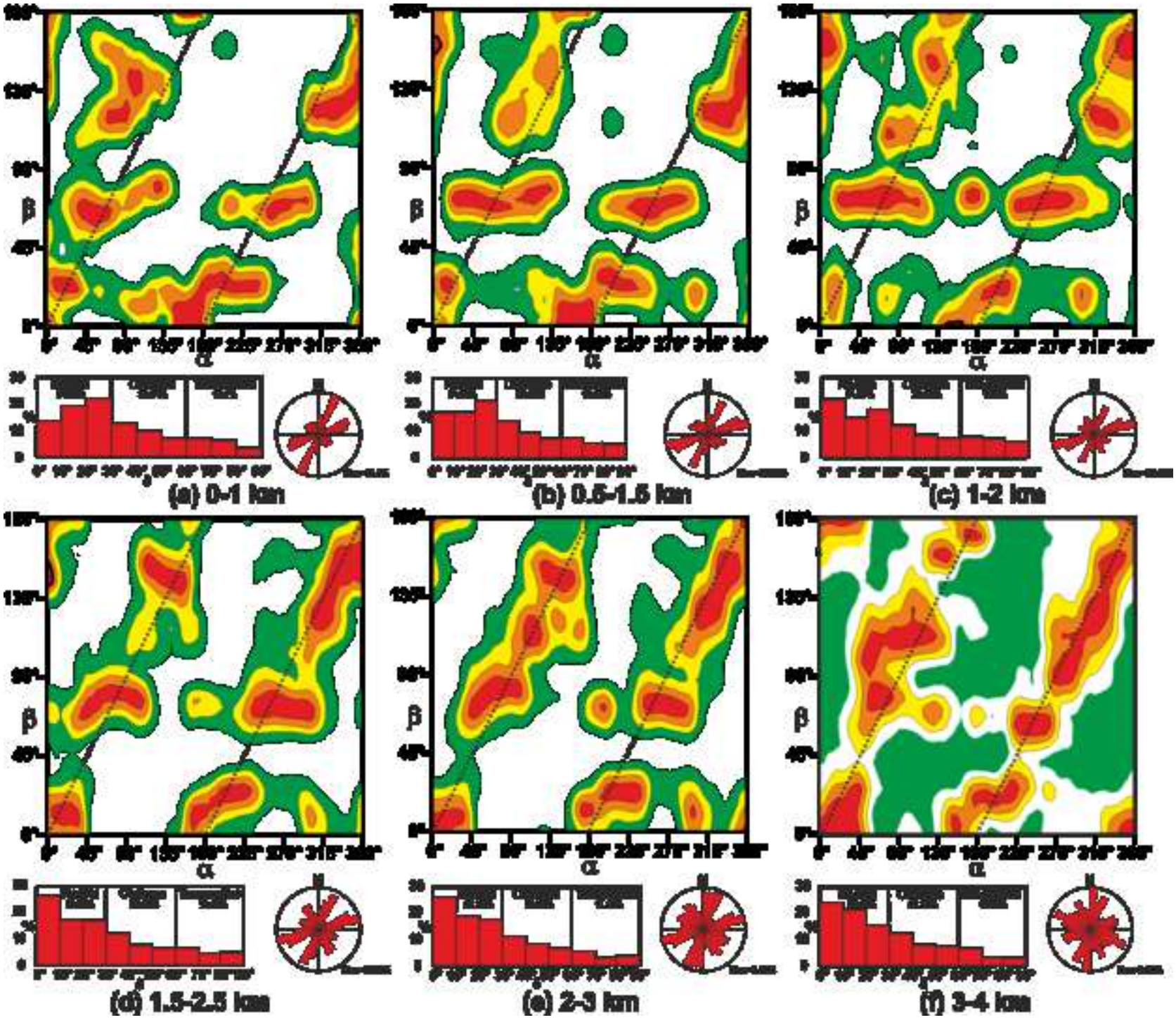

Figure 11

Click here to download Figure Fig. 11.tif